Robust Ghost Imaging Based on Degenerate Spontaneous Parametric Down-Conversion *

Ling-Jun Kong(孔令军)[1], Yu Si(司宇)[1], Rui Liu(刘瑞)[1], Zhou-Xiang Wang(王周祥)[1], Wen-Rong Qi(齐文荣)[1], Chenghou Tu(涂成厚)[1], Yongnan Li(李勇男)[1**], Hui-Tian Wang(王慧田)[1,2,3**]

[1]*School of Physics and Key Laboratory of Weak Light Nonlinear Photonics, Nankai University, Tianjin 300071*
[2]*National Laboratory of Solid State Microstructures and School of Physics, Nanjing University, Nanjing 210093*
[3]*Collaborative Innovation Center of Advanced Microstructures, Nanjing University, Nanjing 210093*

(Received 26 February 2017)

In traditional ghost imaging, the entangled photon pairs produced from the spontaneous parametric down conversion (SPDC) process are used. There is an intrinsic disadvantage that the utilization efficiency of the photon pairs is very low. Inasmuch as all the correlated photon pairs produced by the degenerate SPDC process can be used to record the image of an object, the ghost imaging scheme we present here has a higher utilization efficiency of the photon pairs. We also investigate the robustness of our experimental scheme. The experimental results show that, no matter whether the photon-pair source is two light cones or two beam-like spots, the clear image of the object can be obtained. The slight rotation of the nonlinear crystal has no influence on the imaging quality. Our experimental results also demonstrate that when the part of the photon-pair source in the signal path or the idler path is blocked by unwanted things, the clear ghost image of the object can still be recorded.

PACS: 42.30.Va, 42.65.Lm, 42.30.Wb DOI: 10.1088/0256-307X/34/5/054206

Ghost imaging, as a kind of indirectly imaging technique, was first performed by using entangled two-photon pairs (signal and idler photons) produced from a spontaneous parametric down-conversion (SPDC) process in 1995.[1] In the ghost imaging, the object is illuminated by the signal light, which will be collected by a 'bucket' detector without spatial resolution. The idler light is recorded by a pixelated detector without interaction with the object. The image of the object cannot be directly obtained from either of the two detectors unless coincidence measurement between the signals of the two detectors occurs. Based on this unique process, the ghost imaging has its own inimitable advantages. When the object is located in optically harsh or noisy environments, the image of the object will become blurry with the traditional imaging, but can still be clear with the ghost imaging.[2–4] This unique characteristic makes the ghost imaging be potential in practical applications, such as satellites and aircraft-to-ground-based distant imaging.[5] Its other applications are also reported.[6–9] After the first observation, the ghost imaging has attracted a great deal of attention.[10–13] Many theoretical and experimental works have been carried out.[14–20] Recently, ghost imaging still attracts a great deal of attention. It has been studied with different sources such as an electromagnetic Gaussian Schell model beam,[21] partially coherent vector beam,[22] or with x-Ray.[23,24]

As one important advantage, ghost imaging with entangled light sources possesses a much better visibility of the information naturally,[11,25] compared with the ghost imaging using thermal light sources. In Ref. [26], the polarization-entangled Bell states are used to remove the background associated with the average number of photons and to obtain a higher quality reconstructed image. However, ghost imaging with entangled light sources has two clear disadvantages. One is that the utilization efficiency of the entangled photon pairs is very low, because only one or two intersection points of the two light cones are used for recording the image of the object. The other is that the wave vectors (or the propagation directions) of the entangled photon pairs depend critically on the orientation of the nonlinear crystal. This is to say, a slight rotation of the nonlinear crystal may destroy the imaging quality.

In this Letter, we use the position-correlation photon pairs and a pair of $4f$ systems[10,27] (located in the signal and idler paths) to realize the ghost imaging. In our scheme, no matter what kind of correlated photon-pairs source (beam-like spots or light cones) is used, a clear image of the object can be obtained by utilizing all the photon pairs. What is more, our scheme has no influence on the small rotation of the nonlinear crystal.

In our scheme shown in Fig. 1, the pump light source is a femtosecond (fs) pulsed laser operating at a central wavelength of 405 nm, with a pulse duration of ∼140 fs and a repetition rate of ∼80 MHz. A half-wave plate (HWP) and a polarized beam splitter (PBS) are used to adjust the power of the pump light. Under the condition of degenerate collinear type-I phase matching, the nonlinear crystal (BBO with a dimension of $1\times5\times5\,\mathrm{mm}^3$) will produce the correlated photon pairs with the same polarization and the same wavelength at 810 nm from the degenerate SPDC process.

*Supported by the National Natural Science Foundation of China under Grant Nos 11534006, 11674184 and 11374166, the Natural Science Foundation of Tianjin under Grant No 16JCZDJC31300, and the Collaborative Innovation Center of Extreme Optics.

**Corresponding author. Email: liyongnan@nankai.edu.cn; htwang@nju.edu.cn

© 2017 Chinese Physical Society and IOP Publishing Ltd

The diameter of the collimated pump light beam in the BBO crystal is about 1.8 mm. A dichroic mirror (DM) is used to remove the pump light at 405 nm. A beam splitter (BS) divides the paired photons into two signal and idler paths. In the signal path, two lenses (Ls1 with a focal length of $f = 100$ mm and Ls2 with a focal length of $f = 200$ mm) are used to form a $4f$ system. The center of the BBO crystal is exactly located at the front focal plane of the $4f$ system. The object (O) is located at the back focal plane of the $4f$ system. All the photons passed through the object are collected by a collecting system and then coupled into a multi-mode fiber (MMF) that connects with the single photon detector D1. The arrangement in the idler path is similar to the signal path. In the idler path, a pair of lenses Li1 (with a focal length of $f = 100$ mm) and Li2 (with a focal length of $f = 200$ mm) are used to form the second $4f$ system. Its front focal plane also coincides with the center of the BBO crystal, and its back focal plane is the scanning plane. The end of the other MMF collecting the photons in the idler path is scanned in the scanning X–Y plane. The photons in the idler path, without interaction with the object, are detected by the other single photon detector D2. The image of the object can be obtained with the coincidence measurement between the signals of D1 and D2. The interference filters (IFs) inserted in the signal and idler paths are used to narrow the spectral widths of the signal and idler photons generated from the SPDC process.

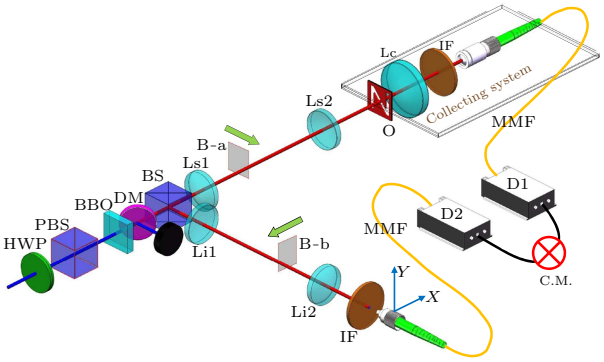

Fig. 1. Experimental scheme of the ghost imaging with two $4f$ systems. DM is a dichroic mirror with a transmission of ∼96% at 810 nm and a reflectivity of ∼97% at 405 nm. B-a and B-b are two screens, which are used to block some parts of the signal and idler light (see text for detail), respectively. The screen B-a is between Ls1 and Ls2. The screen B-b is between Li1 and Li2. Lc is a lens for collecting the photons coming out from the object. IFs are interference filters with a 3-nm bandwidth centered at 810 nm to remove unwanted light. During imaging, the end of the MMF in the idler path will scan in the X–Y plane. The diameter of fiber core is 200 μm for the multi-mode fiber (MMF) connected with detector D1 and is 50 μm for the multi-mode fiber (MMF) connected with detector D2.

In our experiment, the BBO crystal was designed and cut for the degenerate collinear type-I phase matching at the degenerate wavelength of 810 nm, where the pump photons at 405 nm are extraordinarily polarized (e-polarized) and the generated signal and idler photons at the degenerate wavelength of 810 nm are both ordinarily polarized (o-polarized). Under the condition of normal incidence, corresponding to a phase-matching angle $\theta_{m0} = 28.85°$ (in this case, $n_e^p = n_o^s = n_o^i$), the beam-like degenerate photon pairs at 810 nm are generated in the collinear direction of pump ($\boldsymbol{k}^p || \boldsymbol{k}^s || \boldsymbol{k}^i$, $\boldsymbol{k}^s = \boldsymbol{k}^i$, and $|\boldsymbol{k}^p| = |\boldsymbol{k}^s| + |\boldsymbol{k}^i| = 2|\boldsymbol{k}^s| = 2|\boldsymbol{k}^i|$), as shown in Fig. 2(a). For the beam-like photon-pairs generated by the collinear SPDC process, the simulated profile in Fig. 2(b) is in good agreement with the experimentally observed one in Fig. 2(c).

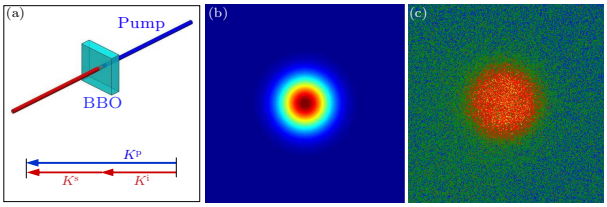

Fig. 2. The distributions of the degenerate photon pairs generated by the SPDC process under the collinear type-I phase matching (the normal incidence). (a) The geometry of the collinear type-I phase matching. (b, c) The distributions of the simulated and experimentally generated photon-pair source.

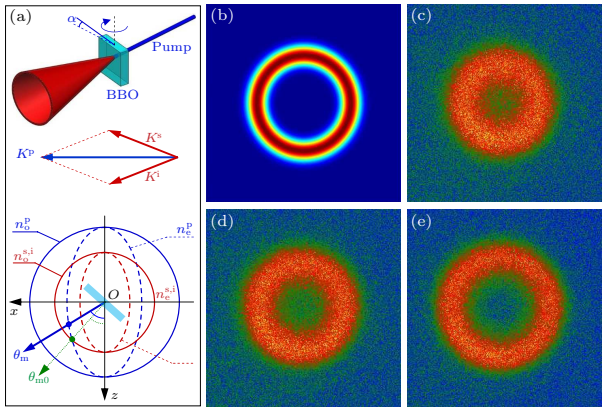

Fig. 3. The distributions of the degenerate photon pairs generated by the SPDC process under the non-collinear type-I phase matching. (a) The geometry of non-collinear type-I phase matching (α is the incident angle or the rotation angle of the BBO crystal), where in the lower diagram the dark-green dotted arrow and the blue arrow indicate the direction of the pump under the collinear and non-collinear type-I phase matching cases, respectively. (b) The simulation result of photon-pair source with $\alpha = 1.5°$. The experimental results of the photon-pair source with $\alpha = 0.5°$ (c), $\alpha = 1.0°$ (d), and $\alpha = 1.5°$ (e).

Under the non-normal incidence (the BBO crystal is rotated in its principal section to change the phase-matching angle θ_m), as shown in Fig. 3(a), although the phase matching becomes non-collinear ($\boldsymbol{k}^p = \boldsymbol{k}^s + \boldsymbol{k}^i$, $\boldsymbol{k}^p \nparallel \boldsymbol{k}^s \nparallel \boldsymbol{k}^i$, and $|\boldsymbol{k}^s| = |\boldsymbol{k}^i|$), the generated signal and idler photon pairs are still degenerate in both wavelength/frequency and light cones. The concentric angle depends on the rotation angle α of the BBO crystal. It should be pointed out that under the condition of $\theta_m = \theta_{m0} + \alpha > \theta_{m0}$ ($\alpha > 0$), the non-collinear phase matching can be satisfied, in contrast, when $\theta_m < \theta_{m0}$ the phase matching can never

be achieved, as shown in Fig. 3(a), based on the reason in the following. When $\theta_{\rm m}$ indicating the propagation direction of the pump is smaller than $\theta_{\rm m0}$ ($\theta_{\rm m} < \theta_{\rm m0}$), the refractive index of the pump becomes larger while that of the signal/idler has no change, $n_{\rm e}^{\rm p} > n_{\rm o}^{s,i}$, thus the phase matching can never be achieved. By contrast, when $\theta_{\rm m} > \theta_{\rm m0}$, the refractive index becomes smaller, $n_{\rm e}^{\rm p} < n_{\rm o}^{\rm s,i}$, the non-collinear phase matching is allowed.

The ghost images of the object can be obtained using different kinds of correlated photon-pair sources, such as beam-like or concentric photon pairs. The experiments of four different conditions (with $\alpha = 0°$, 0.5°, 1.0°, and 1.5°, respectively) have been carried out. Based on the geometric optics, the relationship between the rotation angle α and the concentric angle β, which is the included angle of $\boldsymbol{k}^{\rm s}$ and $\boldsymbol{k}^{\rm i}$ outside the BBO crystal, can be calculated. For $\alpha = 0°$, 0.5°, 1.0°, and 1.5°, the calculation shows $\beta = 0°$, 4.0°, 5.6°, and 6.9°, respectively. The experimental results shown in Fig. 4 demonstrate that no matter which kind of distribution of the photon-pair source is used, a clear image of an object can be obtained. This is to say, a small change in the phase-matching angle of the BBO crystal has no influence on the imaging. When $\alpha \geq 1.5°$, the background of the image becomes stronger, resulting in the decline of contrast in imaging, as shown in Fig. 4(d). The dominant reason is due to the fact that increasing α leads to the larger concentric angle, thus all the photons cannot be collected due to the limited apertures of optical elements used in experiment (Fig. 1).

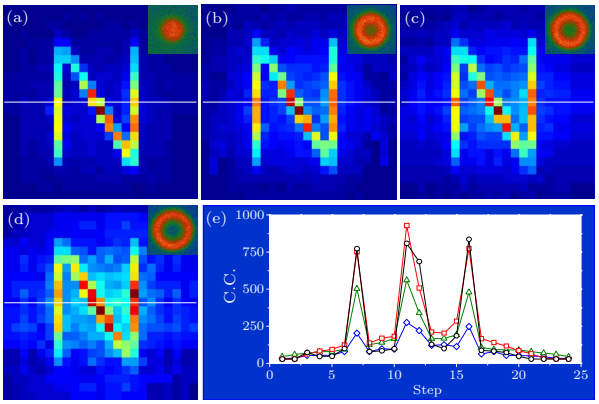

Fig. 4. The ghost images of the object for different kinds of correlated photon-pair sources. (a)–(d) The experimental results of the ghost images reconstructed from the coincidence measurements for $\alpha = 0°$, $\alpha = 0.5°$, $\alpha = 1.0°$, and $\alpha = 1.5°$, respectively. Here $24 \times 24 = 576$ scanning steps are needed for each image. Each step covers 50 μm. (e) The data for calculating the visibility for different kinds of correlated photon-pair sources. The data of the black circles, red squares, green triangles, and blue diamonds correspond to the white line in (a)–(d), respectively. C.C. represents coincidence count in 5 s.

With the data shown Fig. 4(e), the visibilities of the images for different kinds of correlated photon-pair sources in Figs. 4(a)–4(d) are calculated to be $V = 82.5\%$, 74.1%, 63.1%, and 55.6%, respectively, by

$$V = \frac{\langle \text{C.C.} \rangle_{\max} - \langle \text{C.C.} \rangle_{\min}}{\langle \text{C.C.} \rangle_{\max} + \langle \text{C.C.} \rangle_{\min}}.$$

We can see that the change of the incident angle has a slight influence on the visibility and a major impact on the coincidence counting rate.

We explore the influence of the blocking of the signal photons on the quality of the ghost imaging. The experimental results are shown in Fig. 5, for the different blocking with a half, two-thirds and five-sixths of the whole ring. We can find that as long as the blocked part of the signal photons is not larger than five-sixths, a clear ghost image of the object can still be obtained.

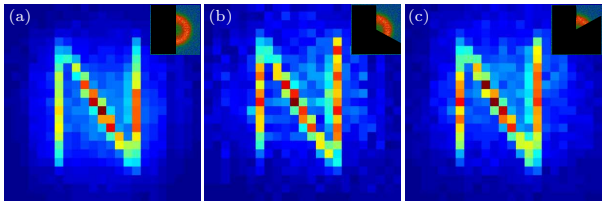

Fig. 5. Ghost images of the object with blocking one part of the signal light beam. (a)–(c) The experimental results of the ghost images of the object with blocking a half, two-thirds, and five-sixths of the whole ring, respectively. The rotation angle of the BBO satisfies $\alpha = 1.0°$.

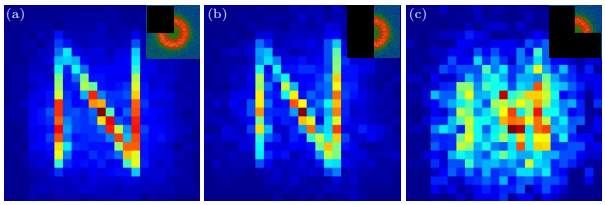

Fig. 6. Ghost images of the object with blocking one part of the idler photons. (a)–(c) The experimental results of the ghost images with the blocking of one-fourth, a half, and three-fourths of the whole ring, respectively. The rotation angle of the BBO crystal is $\alpha = 1.0°$.

We also explore the effect of the blocking of the idler photons. The experimental results are shown in Fig. 6, for the blocking of one-fourth, a half and three-fourths of the whole ring. Our experimental results reveal that when the blocked part is as large as three-fourths (which is different from five-sixths for the signal photons), it is difficult to obtain a clear ghost image of the object. Comparing Fig. 5 with Fig. 6, we can find that the influence of the blocking for the idler photons is stronger than that for the signal photons. A dominant reason is that since the 50-μm core-diameter of MMF used in the idler path is smaller than the 200-μm one of MMF used in the signal path, the idler path is more sensitive to the diffraction effect caused by the screen.

In summery, we have presented a ghost imaging scheme consisting of $4f$ systems in the signal and idler paths. Any $4f$ system composed of a pair of lenses can perfectly image the front focal plane onto the back focal plane. In the SPDC process, each pair of photons are born in the same position inside the non-

linear crystal. The $4f$ system in the signal path will image the plane of the center of the BBO (the plane of the birthplace of a photon-pair) onto the object plane, while the $4f$ system in the idler path will image the plane of the birthplace of the photon pair onto the imaging scanning plane. Thus our scheme can produce a perfect position-correlation photon-pair source. In principle, the properties of the correlation source are independent of the propagation direction of the photon pairs. This is to say, the quality of the correlation source should be independent of the kind of photon-pair sources, which has been demonstrated in our experiment. When the rotation angle of the BBO is $\alpha \geq 1.5°$, all the photons cannot be collected due to the limited apertures of optical elements used in experiment. Thus the background of the image begins to increase. We also demonstrate experimentally that when the blocked part of the signal photons is not larger than five-sixths, a clear ghost image of the object can still be obtained, while the ghost image of the object is still clear when the blocked part of the idler photons is not larger than a half. Therefore, the ghost imaging scheme we present here has not only a robust feature but also a higher utilization efficiency of the photon pairs (a shorter imaging time).

References

[1] Pittman T B, Shih Y H, Strekalov D V and Sergienko A V 1995 *Phys. Rev.* A **52** R3429
[2] Meyers R E, Deacon K S and Shih Y 2012 *Appl. Phys. Lett.* **100** 131114
[3] Meyers R E, Deacon K S and Shih Y 2011 *Appl. Phys. Lett.* **98** 11111
[4] Xue Y L, Wan R G, Feng F and Zhang T Y 2014 *Appl. Opt.* **53** 3035
[5] Li D, Li X, Qin Y and Cheng Y 2014 *IEEE Trans. Geoscience Remote Sensing* **52** 2261
[6] Cheng J 2009 *Opt. Express* **17** 7916
[7] Zhang P L, Gong W L, Shen X and Han S S 2010 *Phys. Rev.* A **82** 033817
[8] Clemente P, Duran V, Torres-Company V, Tajahuerce E and Lancis J 2010 *Opt. Lett.* **35** 2391
[9] Sun B, Edgar M P, Bowman R, Vittert L E, Welsh S, Bowman A and Padgett M J 2013 *Science* **340** 844
[10] Gatti A, Brambilla E, Bache M and Lugiato L A 2004 *Phys. Rev.* A **70** 013802
[11] Gatti A, Brambilla E, Bache M and Lugiato A L 2004 *Phys. Rev. Lett.* **93** 093602
[12] Scarcelli G, Berardi V and Shih Y H 2006 *Phys. Rev. Lett.* **96** 063602
[13] Chan K W C 2012 *Opt. Lett.* **37** 2739
[14] Valencia A, carcelli G, D'Angelo M and Shih Y H 2005 *Phys. Rev. Lett.* **94** 063601
[15] Zhang D, Zhai Y H, Wu L A and Chen X H 2005 *Opt. Lett.* **30** 2354
[16] Kong L J, Li Y N, Qian S X, Li S M, Tu C H and Wang H T 2013 *Phys. Rev.* A **88** 013852
[17] Scarcelli G, Berardi V and Shih Y H 2006 *Appl. Phys. Lett.* **88** 061106
[18] Meyers R, Deacon K S and Shih Y H 2008 *Phys. Rev.* A **77** 041801(R)
[19] Ferri F, Magatti D, Sala V G and Gatti A 2008 *Appl. Phys. Lett.* **92** 261109
[20] Zhou Y, Simon J, Liu J and Shih Y H 2010 *Phys. Rev.* A **81** 043831
[21] Liu X, Wang F, Zhang M and Cai Y 2015 *J. Opt. Soc. Am.* A **32** 910
[22] Tong Z, Cai Y and Korotkova O 2010 *Opt. Commun.* **283** 3838
[23] Pelliccia D, Rack A, Scheel M, Cantelli V and Paganin D M 2016 *Phys. Rev. Lett.* **117** 219902
[24] Yu H, Lu R, Han S, Xie H, Du G, Xiao T and Zhu D 2016 *Phys. Rev. Lett.* **117** 113901
[25] Belinsky A V and Klyshko D N 1992 *Phys. Lett.* A **166** 303
[26] Chirkin A S 2016 *JETP Lett.* **103** 282
[27] Wang X L, Li Y N, Chen J, Guo C S, Ding J P and Wang H T 2010 *Opt. Express* **18** 10786